Nonholonomic Mobile Robots Equipped with Panoramic Cameras: Corridor Following

Dimitris P. Tsakiris and Antonis A. Argyros
Institute of Computer Science - FORTH
Vassilika Vouton, P.O.Box 1385
71110 Heraklion, Crete, Greece
{tsakiris, argyros}@ics.forth.gr
http://www.ics.forth.gr/proj/cvrl

Technical Report ICS TR 272 - JUNE 00

Abstract

The present work considers corridor–following maneuvers for mobile robots with nonholonomic constraints, guided by sensory data acquired by panoramic cameras. The panoramic vision system provides information from an environment with textured walls to the motion control system, which drives the robot along a corridor. Panoramic cameras have a 360° visual field, a capability that the proposed control methods attempt to exploit. We consider two types of sensor–based controllers: one is a path–following state feedback control law where the state of the robot inside the corridor is reconstructed from the visual data; in the other, optical flow information from several distinct "looking" directions in the field of view of the panoramic camera is used directly in the control loop, without the need for state reconstruction. The interest of the second type of controllers lies in the fact that this optical flow information is not sufficient to reconstruct the state of the system, it is however sufficient for the proposed control law to accomplish the desired task. Driving the robot along a corridor amounts to the asymptotic stabilization of a subsystem of the robot's kinematics and the proposed control schemes are shown to achieve this goal.

1 Introduction

Corridor–following maneuvers for mobile robots with nonholonomic constraints are considered, which are guided by sensory data acquired by panoramic cameras. A vision system with a 360° visual field provides information from an environment with textured walls to the motion control system, which drives the robot along a corridor.

The main advantage of panoramic cameras is that they are not constrained by a limited field of view, like classical camera setups. Robotic tasks requiring movement in one direction while observing environmental features in a different one, can then be more easily implemented.

In navigation tasks of mobile robots, the main alternatives to panoramic cameras are moving cameras (e.g. mounted on pan–and–tilt platforms or hand–eye systems) and multiple–camera systems mounted on the robot. In the case of moving cameras, their precise positioning, especially when the mobile robot is also moving, may be a challenging control problem [21]. Looking in a direction outside from the current field of view of the camera, requires repositioning the sensor, which involves a delay that may be unacceptable when the environment also changes. This problem becomes more severe when the direction where the camera needs to look next is not known a–priori; time-consuming exploratory actions are then necessary. In the case of multiple–camera systems, the lack of a common nodal point of the cameras and the elaborate calibration required, complicate their use. The duplication of optical and electronic components increases the cost of the system. Moreover, the system lacks flexibility in observing an arbitrary direction of interest. In contrast to the above, panoramic cameras offer the capability of extracting information simultaneously from all desired directions of their visual field. Neither moving parts, nor elaborate control mechanisms or expensive hardware is required to achieve this capability.

A panoramic image generated by a camera with a paravoloid mirror (like the ones that we consider in this work) can be thought of as a collection of images acquired by ordinary perspective cameras that share a common nodal point. This property simplifies significantly the derivation of the necessary information (Nayar and Baker [13], Svoboda, Pajdla and Hlavac [19]). The advantages of sensors providing a panoramic image, with respect to the solution of the 3D motion estimation problem, are also well known (Fermüller and Aloimonos [7]). These advantages of wide field–of–view images significantly benefit navigation tasks; in contrast, a narrow field–of–view image, corresponding e.g. to the human frontal eye positioning, appears to benefit the manipulation capabilities of the system.

Biological systems are known to exploit wide field–of–view images in controlling their motion. The velocity of the perceived relative motion between the moving biological observer and its environment (optical flow), inferred from such image sequences, can be used to control the motion of the observer. Bees, for example, have laterally–pointing eyes, which amounts to a wide f.o.v., and use optical flow from such images to infer distance flown and control their flight (Collett [5], Srinivasan, Zhang, Altwein and Tautz [18]).

Sensor–based control strategies for robotic systems are well developed for manipulator arms; visual servoing, for instance, which consists in the direct use of visual information in a system's control loop (Espiau, Chaumette and Rives [6], Hager and Hutchinson [9]), provides relatively simple and robust solutions to various positioning and tracking tasks. Their exten-

sion to the case of mobile robots is of significant importance for practical applications (e.g. in automating car driving maneuvers). However, it becomes complicated by the presence of nonholonomic kinematic constraints in the motion of the mobile base, necessitating the use of nonlinear control analysis and design tools (Tsakiris, Samson and Rives [20], [21]).

Vision–based path–following tasks, similar to ours and using wide f.o.v. sensor arrangements are considered in Santos–Victor, Sandini, Curotto and Garibaldi [15], Argyros and Bergholm [1] and Gaspar and Santos–Victor [8]. In [15], a two–camera system is considered, which is mounted on a mobile robot, with the cameras facing opposite lateral directions. The disparity between the average optical flow from the cameras is used in a PID loop controlling the angular velocity of the robot, while this moves at constant speed along a wall. In [1], the normal flow field (the component of optical flow along the image gradients) from a particular arrangement of three perspective cameras guides a path–following task. An important difference of this work with the present one, which employs a panoramic camera, is that processing of images is now significantly simplified by avoiding the need for calibration of a multi–camera setup and by exploiting the properties of panoramic images. In [8], a landmark–based method for the reconstruction of the pose of a mobile robot from panoramic images is presented. The reconstructed pose is, then, fed into the nonlinear state–feedback path–following scheme developed in Samson [16], [17]. From the image understanding viewpoint, this reconstruction is a relatively difficult and error–prone procedure, which we attempt to bypass in our scheme. These works do not attempt, in general, a stability analysis of the resulting control scheme.

The task that we attempt to accomplish amounts to the asymptotic stabilization of a subsystem of the robot's kinematics. Optical flow information from several distinct viewing directions is used. After being derotated, it provides an estimate of the scaled difference of inverse depths in these directions. Our sensor–based control scheme employs this estimate directly in the control loop, without reconstructing the state of the system. This is very much in the spirit of visual servoing schemes. The resulting control law is shown, using Lyapunov's indirect method, to possess the necessary asymptotic stability properties, in the cases that the heading speed of the mobile robot varies with time, but remains strictly positive or negative over the entire duration of the task, and in the case that it varies periodically.

2 Preliminaries

This section summarizes some stability concepts and methods needed in the sequel. Further details can be found in Khalil [12] and Vidyasagar [22].

Definition 1 *(Stability of Autonomous Systems)*
Consider the autonomous system

$$\dot{x}(t) = f[x(t)] \; , \tag{1}$$

where $f : I\!R^n \longrightarrow I\!R^n$ *is locally Lipschitz. Let* $x(t)$ *be the solution of system 1 at time* t*, corresponding to the initial condition* $x(0)$*. Assume that* $x = 0$ *is an equilibrium of system 1, i.e.* $f(0) = 0$*. Then this equilibrium is:*

- Stable, *if for each* $\epsilon > 0$*, there is a* $\delta = \delta(\epsilon)$ *such that, if* $||x(0)|| < \delta$*, then* $||x(t)|| < \epsilon$*,* $\forall\, t \geq 0$*.*
- Asymptotically Stable, *if it is stable and there exists a* $c > 0$ *such that, if* $||x(0)|| < c$*, then* $\lim_{t\to\infty} x(t) = 0$*.*
- Unstable, *if it is not stable.*

Thus, when the nonlinear system 1 is stable, for any ϵ–neighborhood of the origin there is a δ–neighborhood of it, such that a trajectory starting in the latter never leaves the former.

Definition 2 *(Stability of Non–autonomous Systems)*
Consider the non–autonomous system

$$\dot{x}(t) = f[t, x(t)] \; , \tag{2}$$

where $f : [0,\ \infty) \times I\!R^n \longrightarrow I\!R^n$ *is piecewise continuous in* t *and locally Lipschitz in* x *on* $[0,\ \infty) \times I\!R^n$*. Let* $x(t)$ *be the solution of system 2 at time* t*, corresponding to the initial condition* $x(0)$*. Assume that* $x = 0$ *is an equilibrium of system 2 at time* 0*, i.e.* $f(t,\ 0) = 0,\ \forall\, t \geq 0$*. Then this equilibrium is:*

- Stable, *if for any* $\epsilon > 0$ *and* $t_0 \geq 0$*, there is a* $\delta = \delta(t_0, \epsilon) > 0$ *such that, if* $||x(t_0)|| < \delta(t_0, \epsilon)$*, then* $||x(t)|| < \epsilon$*,* $\forall\, t \geq t_0$*.*
- Uniformly stable *over* $[0,\ \infty)$*, if for any* $\epsilon > 0$*, there is a* $\delta = \delta(\epsilon)$ *such that, if* $||x(t_0)|| < \delta(\epsilon)$ *for* $t_0 \geq 0$*, then* $||x(t)|| < \epsilon$*,* $\forall\, t \geq t_0 \geq 0$*.*
- Asymptotically stable, *if it is stable and if, for any* $t_0 \geq 0$*, there exists a* $\delta = \delta(t_0) > 0$ *such that, if* $||x(0)|| < \delta(t_0)$*, then* $\lim_{t\to\infty} x(t) = 0$*.*
- Uniformly asymptotically stable *over* $[0,\ \infty)$*, if it is uniformly stable over* $[0,\ \infty)$ *and there exists a* $\delta > 0$*, independent of* t_0*, such that, if* $||x(t_0)|| < \delta$ *for* $t_0 \geq 0$*, then* $\lim_{t\to\infty} x(t) = 0$ *and the convergence is uniform in* t_0 *(i.e. for any* $\epsilon > 0$*, there is a* $T(\epsilon) < \infty$*, independent of* t_0*, such that, if* $||x(t_0)|| < \delta$*, then* $||x(t)|| < \epsilon$*, whenever* $t > t_0 + T(\epsilon)$ *)* .

- Exponentially Stable, *if there exist constants* $c > 0,\ k > 0$ *and* $\gamma > 0$, *such that, if* $||x(t_0)|| < \delta$ *for* $t_0 \geq 0$, *then* $||x(t)|| \leq k\ ||x(t_0)||\ e^{-\gamma(t-t_0)},\ \forall\ t \geq t_0 \geq 0$.
- Unstable, *if it is not stable.*

Proposition 1 *(Lyapunov's indirect method) [22]*
Consider the non–autonomous system

$$\dot{x}(t) = f[t, x(t)]\ , \tag{3}$$

where $f(t, \cdot)$ *is continuously differentiable and* $f(t, 0) = 0$.
Define

$$\begin{aligned} A(t) &\stackrel{\text{def}}{=} \left[\frac{\partial f}{\partial x}(t, x)\right]_{x=0}\ , \\ f_1(t, x) &\stackrel{\text{def}}{=} f(t, x) - A(t)\ x \end{aligned} \tag{4}$$

and assume that $A(\cdot)$ *is bounded and that*

$$\lim_{||x|| \to 0}\ \sup_{t \geq 0} \frac{||f_1(t, x)||}{||x||} = 0\ . \tag{5}$$

Then, if the equilibrium $z = 0$ *of the system*

$$\dot{z}(t) = A(t) z(t) \tag{6}$$

is uniformly asymptotically stable over $[0, \infty)$, *the equilibrium* $x = 0$ *of the system 3 is also uniformly asymptotically stable over* $[0, \infty)$.

The system 6 is called the *linearization* of the nonlinear system 3 around the equilibrium $x = 0$.

3 Modeling

3.1 Mobile Robot Modeling

We consider a mobile robot of the unicycle type moving on a planar surface inside a corridor with straight parallel textured walls. We suppose that a panoramic camera is mounted on the robot (fig. 1).

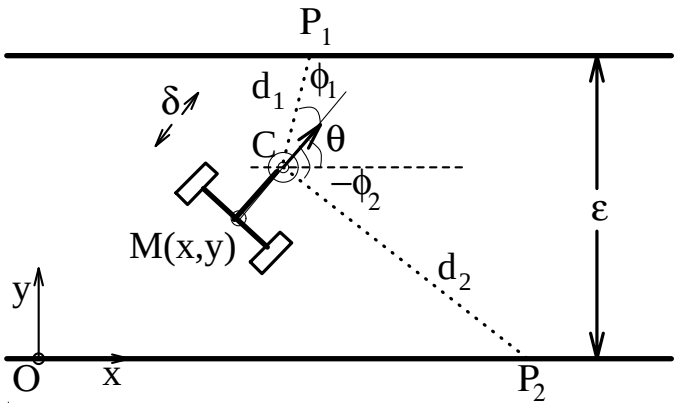

Figure 1: Mobile Robot with Panoramic Camera

Consider an inertial coordinate system $\{F_O\}$ centered at a point O of the plane and aligned with one of the walls, a moving coordinate system $\{F_M\}$ attached to the middle M of the robot's wheel axis and another moving one $\{F_C\}$ attached to the nodal point C of the camera. Let (x, y) be the position of the point M and θ be the orientation of the mobile robot with respect to the coordinate system $\{F_O\}$. Let δ be the distance of the point C from M and ϵ the width of the corridor.

We suppose that the wheels of the mobile platform roll without slipping on the plane supporting the system. This induces a nonholonomic constraint on the motion of the mobile robot, due to the fact that the instantaneous velocity lateral to the heading direction of the mobile platform has to be zero. From this, we get the usual unicycle kinematic model for the mobile platform

$$\dot{x} = v\cos\theta \ , \quad \dot{y} = v\sin\theta \ , \quad \dot{\theta} = \omega \ , \tag{7}$$

where $v \stackrel{\text{def}}{=} \dot{x}\cos\theta + \dot{y}\sin\theta$ is the heading speed and ω is the angular velocity of the unicycle.

3.2 Panoramic Camera Modeling

Consider a pinhole camera and a camera-centered coordinate system $CXYZ$ positioned at its optical center C, with the CZ axis coinciding with the optical axis. Assume that the camera is moving rigidly with respect to its 3D static environment with translational velocity (U, V, W) and rotational velocity (α, β, γ), both expressed with respect to the camera coordinate system. Under perspective projection, the relation between the 2D velocity $(u^x,\ u^y)$ of an image point p with image coordinates (x, y) and the 3D velocity of the corresponding 3D point P with coordinates (X, Y, Z) is given by the optical flow equations [11]

(a) Original panoramic image

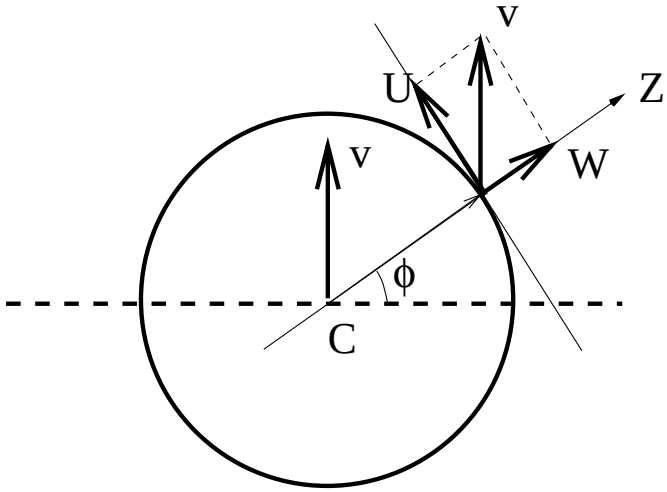

(b) Panoramic camera geometry

(c) Corresponding unfolded cylindrical image

Figure 2: Panoramic Image

$$u^x = \frac{-Uf + xW}{Z} + \alpha\frac{xy}{f} - \beta\left(\frac{x^2}{f} + f\right) + \gamma y \ , \quad u^y = \frac{-Vf + yW}{Z} + \alpha\left(\frac{y^2}{f} + f\right) - \beta\frac{xy}{f} - \gamma x \ , \tag{8}$$

where f is the focal length of the pinhole camera. Consider a mobile robot of the type described above, with a panoramic camera mounted on it, so that the symmetry axis of the paravoloid mirror passes through the robot's axis of rotation (in the notation of fig. 1, this corresponds to $\delta = 0$.)

The panoramic image can be "unfolded" giving rise to a cylindrical image. An example of a panoramic image and the resulting cylindrical image is shown in fig. 2. Different columns of the resulting cylindrical image correspond to different viewing directions in the range $[0,\ 2\pi]$. We suppose that the heading direction of the robot is the one recorded on the cylindrical image column that corresponds to $\pi/2$ (fig. 2.b).

The resulting cylindrical images can be approximated by a number of perspective images that have no overlapping visual fields and which are tangent to the cylindrical surface. The approximation becomes more accurate as the number of images increases and their corresponding visual fields become smaller. In the extreme case, these images become one–dimensional vertical arrays of pixels corresponding to the columns of the cylindrical image.

For these "virtual" perspective images we may employ equations 8 to analyze the flow generated due to the robot's motion. More specifically, consider the column of the cylindrical image which corresponds to the viewing direction ϕ. Suppose that the part of the 3D scene

projected on this column lies in depth d. The heading speed v of the robot results in two components of translational velocity in the image coordinate system: $W = v \sin\phi$ and $U = v \cos\phi$ (see fig. 2.b). Since we consider a robot that moves on a planar surface, the vertical component V of the camera's translational velocity becomes zero. Regarding the rotational velocity, only $\beta = \omega$ is non–zero. By taking into account the above considerations, as well as the fact that $x \approx 0$ in the local coordinate systems of all "virtual" perspective cameras, equations 8 become:

$$u^x_\phi = -\frac{v\ f \cos\phi}{d} - \omega f\ , \quad u^y_\phi = \frac{y\ v \sin\phi}{d}\ . \tag{9}$$

In the heading direction of the robot ($\phi = \pi/2$), the horizontal component of the optical flow u^x_h is equal to $-\omega f$, i.e. it depends only on the rotational component of the robot's motion.

Suppose now that we measure (cf. Hildreth [10], Horn [11], Barron, Fleet and Beauchemin [2], and references therein) the horizontal component of the optical flow $u^x_{\phi_1}$ and $u^x_{\phi_2}$ in two different directions ϕ_1 and ϕ_2, respectively, with corresponding depths d_1 and d_2. Define the following quantities:

$$\mathcal{L}_1 \stackrel{\text{def}}{=} u^x_{\phi_1} + u^x_{\phi_2} - 2\ u^x_h\ , \quad \mathcal{L}_2 \stackrel{\text{def}}{=} u^x_{\phi_1} - u^x_{\phi_2}\ . \tag{10}$$

It can be easily verified that

$$\mathcal{L}_1 = -v\ f\ (\frac{\cos\phi_1}{d_1} + \frac{\cos\phi_2}{d_2})\ , \quad \mathcal{L}_2 = -v\ f\ (\frac{\cos\phi_1}{d_1} - \frac{\cos\phi_2}{d_2})\ . \tag{11}$$

The depths d_1 and d_2 can, then, be specified from $\mathcal{L}_1$ and $\mathcal{L}_2$, which are measured from visual data, provided that the heading speed v is known or can be estimated:

$$d_1 = -2v\ f\frac{\cos\phi_1}{\mathcal{L}_1 + \mathcal{L}_2}\ , \quad d_2 = -2v\ f\frac{\cos\phi_2}{\mathcal{L}_1 - \mathcal{L}_2}\ . \tag{12}$$

Notice that in the case that the directions ϕ_1 and ϕ_2 are arranged symmetrically about the heading direction of robot, the quantity $\mathcal{L}_1$ allows the estimation of the scaled difference of inverse depths. Indeed, let $\phi_1 = \frac{\pi}{2} + \phi$ and $\phi_2 = \frac{\pi}{2} - \phi$, with $\phi \in (0,\ \frac{\pi}{2})$. Then $\cos\phi_1 = -\cos\phi_2 = -\sin\phi$, and

$$\mathcal{L}_1 = v\ f \sin\phi\ (\frac{1}{d_1} - \frac{1}{d_2})\ , \quad \mathcal{L}_2 = v\ f \sin\phi\ (\frac{1}{d_1} + \frac{1}{d_2})\ . \tag{13}$$

The quantity $\mathcal{L}_1$ is shown to be sufficient for controlling the robot during a corridor–following behavior, without the need for full reconstruction of the robot's state.

A significant advantage of using a panoramic camera for such a task is that the "looking direction" ϕ, which is used in computing the quantities $\mathcal{L}_1$ and $\mathcal{L}_2$ above, can be changed in software in a simple way or can be made to vary over a range of values.

3.3 Reconstruction of the state y and θ

Consider the rays d_1 and d_2 in the "forward" directions ϕ and $-\phi$ and the rays d_3 and d_4 in the "backwards" directions $-(\pi - \phi)$ and $\pi - \phi$, with respect to the heading direction of the

robot (fig. 1). We suppose that d_1 and d_4 intersect the left wall, while d_2 and d_3 intersect the right wall of the corridor. The magnitudes of the rays (depths) are related to the parameters of the system and to the state of the robot as follows:

$$d_1 = \frac{\epsilon - y - \delta \sin\theta}{\sin(\theta+\phi)} \ , \quad d_2 = -\frac{y + \delta \sin\theta}{\sin(\theta-\phi)} \ , \quad d_3 = \frac{y + \delta \sin\theta}{\sin(\theta+\phi)} \ , \quad d_4 = -\frac{\epsilon - y - \delta \sin\theta}{\sin(\theta-\phi)} \ . \quad (14)$$

We suppose that $y \in (0,\ \epsilon)$ and $\theta \in (-\phi,\ \phi)$, with $0 < \phi < \frac{\pi}{2}$. Thus, $\sin(\theta+\phi) \neq 0$ and $\sin(\theta-\phi) \neq 0$. When $y = y_\star \stackrel{\text{def}}{=} \frac{\epsilon}{2}$ and $\theta = \theta_\star \stackrel{\text{def}}{=} 0$, we have $d_i = d_{i,\star} \stackrel{\text{def}}{=} \frac{\epsilon}{2 \sin\phi}$, for $i = 1, \ldots, 4$.

The depths $d_i,\ i = 1, \ldots, 4$, can be specified from optical flow using equations 11. By measuring optical flow in the "forward" directions ϕ and $-\phi$ with respect to the heading direction of robot (i.e. by setting $\phi_1 = \frac{\pi}{2} + \phi$ and $\phi_2 = \frac{\pi}{2} - \phi$), we get $\cos\phi_1 = -\cos\phi_2 = -\sin\phi$, thus

$$\mathcal{L}_1^{1,2} \stackrel{\text{def}}{=} u^x_{\phi_1} + u^x_{\phi_2} - 2\ u^x_h = v\ f \sin\phi\ (\frac{1}{d_1} - \frac{1}{d_2}) \ , \quad \mathcal{L}_2^{1,2} \stackrel{\text{def}}{=} u^x_{\phi_1} - u^x_{\phi_2} = v\ f \sin\phi\ (\frac{1}{d_1} + \frac{1}{d_2}) \ . \quad (15)$$

Then

$$d_1 = -2v\ f \frac{\cos\phi_1}{\mathcal{L}_1^{1,2} + \mathcal{L}_2^{1,2}} = 2v\ f \frac{\sin\phi}{\mathcal{L}_1^{1,2} + \mathcal{L}_2^{1,2}} \ , \quad d_2 = -2v\ f \frac{\cos\phi_2}{\mathcal{L}_1^{1,2} - \mathcal{L}_2^{1,2}} = -2v\ f \frac{\sin\phi}{\mathcal{L}_1^{1,2} - \mathcal{L}_2^{1,2}} \ . \quad (16)$$

By measuring optical flow in the "backwards" directions $-(\pi-\phi)$ and $\pi-\phi$ with respect to the heading direction of robot (i.e. setting $\phi_3 = -\frac{\pi}{2} + \phi$ and $\phi_4 = -\frac{\pi}{2} - \phi$), we get $\cos\phi_3 = -\cos\phi_4 = \sin\phi$, thus

$$\mathcal{L}_1^{3,4} \stackrel{\text{def}}{=} u^x_{\phi_3} + u^x_{\phi_4} - 2\ u^x_h = -v\ f \sin\phi\ (\frac{1}{d_3} - \frac{1}{d_4}) \ , \quad \mathcal{L}_2^{3,4} \stackrel{\text{def}}{=} u^x_{\phi_3} - u^x_{\phi_4} = -v\ f \sin\phi\ (\frac{1}{d_3} + \frac{1}{d_4}) \ . \quad (17)$$

Then

$$d_3 = -2v\ f \frac{\cos\phi_3}{\mathcal{L}_1^{3,4} + \mathcal{L}_2^{3,4}} = -2v\ f \frac{\sin\phi}{\mathcal{L}_1^{3,4} + \mathcal{L}_2^{3,4}} \ , \quad d_4 = -2v\ f \frac{\cos\phi_4}{\mathcal{L}_1^{3,4} - \mathcal{L}_2^{3,4}} = 2v\ f \frac{\sin\phi}{\mathcal{L}_1^{3,4} - \mathcal{L}_2^{3,4}} \ . \quad (18)$$

Given the depths $d_i,\ i = 1, \ldots, 4$, that can be specified from optical flow as described above, we want to find y and θ.

We first consider reconstructing θ. By "looking" in the forward direction (i.e. by using the rays d_1 and d_2), we get from equations 14:

$$\begin{aligned} \theta &= 2 \arctan\left(\frac{(d_1 - d_2)\cos\phi \pm \sqrt{d_1^2 + d_2^2 - 2 d_1 d_2 \cos(2\phi) - \epsilon^2}}{\epsilon + (d_1 + d_2)\sin\phi} \right) \\ &= \arcsin\left(\frac{\epsilon}{\sqrt{(d_1+d_2)^2 - 4 d_1 d_2 \cos^2\phi}} \right) - \arctan\left(\frac{d_1 + d_2}{d_1 - d_2} \tan\phi \right) . \end{aligned} \quad (19)$$

As $\theta \in (-\frac{\pi}{2}, \frac{\pi}{2})$, the above expressions (19) provide two solutions θ, one of which has to be selected. Similar expressions are derived if we reconstruct θ by "looking" backwards (i.e. by using the rays d_3 and d_4).

If we "look" sideways (i.e. use the rays d_1 and d_4 or d_2 and d_3), we get, in each case, a single solution θ from the equations 14:

$$\theta = \arctan\left(\frac{d_2 - d_3}{d_2 + d_3}\tan\phi\right) = \arctan\left(\frac{d_4 - d_1}{d_4 + d_1}\tan\phi\right) . \tag{20}$$

As $-\frac{\pi}{2} < \theta < \frac{\pi}{2}$, each of the two functions in equation 20 returns a unique value in this interval.

To increase robustness in the presence of noisy visual data, all possible pairs of rays can be used to provide estimates of θ and the median of these can be used as the final estimate.

Another method consists in reconstructing θ from two different "forward" directions ϕ_1 and ϕ_2

$$\theta = \arctan\left(\frac{d_{1,2}\sin\phi_2 - d_{1,1}\sin\phi_1}{d_{1,1}\cos\phi_1 - d_{1,2}\cos\phi_2}\right) = \arctan\left(\frac{d_{2,1}\sin\phi_1 - d_{2,2}\sin\phi_2}{d_{2,1}\cos\phi_1 - d_{2,2}\cos\phi_2}\right) , \tag{21}$$

where $d_{1,j}$, $d_{2,j}$ are depths in the "forward" direction ϕ_j.

Knowing θ, we can estimate y from equation 14 in several ways, some of which are indicated here:

$$\begin{aligned} y &= -\delta\sin\theta - d_2\sin(\theta - \phi) \\ &= \frac{1}{2}\Big[-2\delta\sin\theta + d_3\sin(\theta + \phi) - d_2\sin(\theta - \phi)\Big] \\ &= \frac{1}{2}\Big[\epsilon - 2\delta\sin\theta - d_1\sin(\theta + \phi) - d_2\sin(\theta - \phi)\Big] . \end{aligned} \tag{22}$$

4 Motion Control

4.1 The Task: Corridor Following

The task of following a straight–line corridor consists of using the angular velocity of the system to drive the lateral distance of the robot from the walls, as well as its orientation, to desired values. This amounts to asymptotically stabilizing the state (y, θ) of the subsystem

$$\dot{y} = v \sin\theta \ , \quad \dot{\theta} = \omega \tag{23}$$

of the unicycle kinematics 7 to $(y_\star,\ \theta_\star)$, using only the angular velocity ω as the control of the system. The heading speed $v(t)$ cannot be controlled, but we suppose that it is known at all times (e.g. it is measured from odometry, vision, etc.).

4.2 Motion Control under Complete State Information

In the case that reconstruction of the state (y, θ) from the panoramic camera data is possible, a path-following control scheme similar to the one developed by Samson [16] (cf. also Ch. 9 of [4]) can be applied to the system. The heading speed v is allowed to vary with time, but we suppose that it is bounded, that its time derivative $\dot{v}$ is also bounded and that v does not tend asymptotically to zero. Then, the angular velocity

$$\omega = -k_1\ \tilde{y}\ \frac{\sin\tilde{\theta}}{\tilde{\theta}}\ v - k_2\ \tilde{\theta}\ |v| \ , \tag{24}$$

with $\tilde{\theta} = \theta - \theta_\star$ and $\tilde{y} = y - y_\star$ and with positive $k_1,\ k_2$, which satisfy the stability requirements for the corresponding linearized system, can be used to asymptotically stabilize the system 23 to $(y_\star,\ \theta_\star)$. This can be shown by Lyapunov analysis (Samson [16], [4]).

4.3 Motion Control under Incomplete State Information

We saw previously that the quantities

$$\mathcal{L}_1^{1,2} = u_1^x + u_2^x - 2u_h^x = v\ f \sin\phi\ (\frac{1}{d_1} - \frac{1}{d_2}) \tag{25}$$

and

$$\mathcal{L}_1^{3,4} = u_3^x + u_4^x - 2u_h^x = -v\ f \sin\phi\ (\frac{1}{d_3} - \frac{1}{d_4}) \ , \tag{26}$$

with $\phi \in (0,\ \frac{\pi}{2})$, can be directly extracted from the panoramic camera data by "looking" at a total of five distinct directions (namely, by calculating optical flow in these directions). At every time instant we calculate either $\mathcal{L}_1^{1,2}$ from "forward–looking" data or $\mathcal{L}_1^{3,4}$ from "backwards–looking" data. Either one of these quantities is not sufficient for a full reconstruction of the state (y, θ). It is of interest however to consider whether they suffice for the accomplishment of the path following task described above.

In the case that v is time–varying, but strictly positive $(v(t) > 0, \forall t \geq 0)$, the angular velocity control $\omega_1 = -k_1\ \mathcal{L}_1^{1,2}$, with positive gain k_1, can be shown to locally asymptotically

stabilize the system 23 to $(y_\star,\ \theta_\star)$. When v is piecewise continuous, bounded and positive at all times, an input scaling procedure [17] can be used to reduce the linearization of the closed–loop system around the desired equilibrium to a linear time–invariant system, whose asymptotic stability can be established by classical results like the Routh–Hurwitz test. Linear theory tools can also be employed to select the gain k_1 (e.g. for critical damping of the trajectory).

In the case that v is strictly negative, and even if it is constant, controlling the system 23 by ω_1 above, will lead to instability. Indeed, the linearization of the closed–loop system can be shown to possess eigenvalues with positive real part and, by Lyapunov's indirect method, the instability of the corresponding nonlinear system is deduced. Therefore, a different control law is required.

In the case that v is time–varying, but strictly negative ($v(t) < 0, \forall t \geq 0$), the angular velocity control $\omega_2 = -k_2\ \mathcal{L}_1^{3,4}$, with positive gain k_2, can be shown to locally asymptotically stabilize the system 23 to $(y_\star,\ \theta_\star)$. Also, if ω_2 above is applied to the system in the case when v is strictly positive and constant, the system becomes unstable.

Proposition 2 *(Asymptotic Stability when $v(t) > 0$)*

Let the heading speed v of the unicycle 7 be time–varying and assume that it is strictly positive at all times, piecewise continuous and bounded. Let d_1 and d_2 be the distances from the panoramic camera to the walls of the corridor in directions ϕ and $-\phi$ with respect to the heading of the unicycle. The angular velocity

$$\omega_1 = -k_1\ \mathcal{L}_1^{1,2}\ , \tag{27}$$

with gain $k_1 > 0$, stabilizes locally asymptotically the subsystem 23 of the unicycle kinematics to $(y_\star,\ \theta_\star) = (\frac{\epsilon}{2},\ 0)$.

Proof

The closed–loop system is

$$\begin{aligned} \dot{y} &= v \sin\theta\ , \\ \dot{\theta} &= \omega_1 = -k_1\ v\ f \sin\phi\ (\frac{1}{d_1} - \frac{1}{d_2}) = -k_1\ v\ f \sin\phi\ \left[\frac{\sin(\theta+\phi)}{\epsilon - y - \delta\sin\theta} + \frac{\sin(\theta-\phi)}{y + \delta\sin\theta}\right]\ . \end{aligned} \tag{28}$$

The linearization of the closed–loop system around $(y_\star,\ \theta_\star)$ is

$$\dot{z} = A_1(v)\ z \stackrel{\text{def}}{=} \begin{pmatrix} 0 & v \\ -k_1 v \alpha_1 & -k_1 v \alpha_2 \end{pmatrix} z\ , \tag{29}$$

where $z \stackrel{\text{def}}{=} (z_2, z_3) \stackrel{\text{def}}{=} (y - y_\star,\ \theta - \theta_\star)$, $\alpha_1 \stackrel{\text{def}}{=} 8 f \frac{\sin^2\phi}{\epsilon^2} > 0$ and $\alpha_2 \stackrel{\text{def}}{=} 4 f \frac{\sin\phi}{\epsilon^2}(\epsilon\cos\phi + 2\delta\sin\phi) > 0$. (N.B. we suppose that $\phi \in (0,\ \frac{\pi}{2})$).

In 29 we replace differentiation with respect to time t by differentiation with respect to the variable s defined by $\dot{s} \stackrel{\text{def}}{=} \frac{ds}{dt} = |v(t)|$. Since v is piecewise continuous, bounded and positive at all times, s is strictly monotonic. Therefore, for a function $f(t)$:

$$\frac{df}{dt} = \frac{df}{ds}\frac{ds}{dt} = \frac{df}{ds} v\ . \tag{30}$$

Differentiating z with respect to s, we get from 29 and 30:

$$\frac{dz}{ds} = A_2\, z \stackrel{\text{def}}{=} \begin{pmatrix} 0 & 1 \\ -k_1\alpha_1 & -k_1\alpha_2 \end{pmatrix} z \ , \tag{31}$$

The time–varying linear system 29 is now transformed into a time–invariant one, whose stability can be analyzed by the Routh–Hurwitz test. The corresponding characteristic polynomial is

$$\det(s\mathit{I\!I} - A_2) = s^2 + k_1\alpha_2 s + k_1\alpha_1 \ , \tag{32}$$

where $\mathit{I\!I}$ is the 2×2 identity matrix. The elements of the first column of the Routh array are 1, $k_1\alpha_2$, $k_1\alpha_1$, all of which are positive. Thus, all roots of the characteristic polynomial are in the left half plane.

Therefore, from Lyapunov's indirect method, the system 28 is asymptotically stable around $(y_\star,\ \theta_\star)$.

∎

Analysis of the second–order time–invariant linear system 31 shows that its natural undamped frequency is $\omega_n = \sqrt{k_1\alpha_1}$ and its damping ratio is $\zeta = \sqrt{k_1}\frac{\alpha_2}{2\sqrt{\alpha_1}}$. Critical damping is achieved for $\zeta = 1$, thus for

$$k_1 = \frac{4\alpha_1}{\alpha_2^2} = \frac{2\epsilon^2}{f(\epsilon\cos\phi + 2\delta\sin\phi)^2} \ . \tag{33}$$

This can be used as a guideline in selecting the gain of the control ω_1.

Proposition 3 *(Instability when $v(t) > 0$)*

Assume that the heading speed v of the unicycle 7 is strictly negative and constant. The angular velocity ω_1 of 27 makes the subsystem 23 of the unicycle kinematics unstable.

Proof

As in the previous proof, after linearization of the closed–loop system 28, we obtain the linear system 29. However, since we now consider constant v, this is a time–invariant system. Its characteristic polynomial is

$$\det(s\mathit{I\!I} - A_1) = s^2 + k_1 v\alpha_2 s + k_1 v^2\alpha_1 \ . \tag{34}$$

The elements of the first column of the Routh array are 1, $k_1 v\alpha_2$ (< 0), $k_1 v^2\alpha_1$ (> 0). There are two sign changes in these elements, thus there are two roots of the characteristic polynomial with positive real parts. Therefore, from Lyapunov's indirect method, the system 28 is unstable.

∎

Proposition 4 *(Asymptotic Stability when $v(t) < 0$)*

Let the heading speed v of the unicycle 7 be time–varying and assume that it is strictly negative at all times, piecewise continuous and bounded. Let d_3 and d_4 be the distances from

the panoramic camera to the walls of the corridor in directions $-(\pi-\phi)$ *and* $(\pi-\phi)$ *with respect to the heading of the unicycle. If* $\epsilon\cos\phi - 2\delta\sin\phi > 0$, *the angular velocity*

$$\omega_2 = -k_2\ \mathcal{L}_1^{3,4}\ , \tag{35}$$

with gain $k_2 > 0$, *stabilizes locally asymptotically the subsystem 23 of the unicycle kinematics to* $(y_\star,\ \theta_\star)$.

Proof

The closed–loop system is

$$\begin{aligned} \dot{y} &= v\sin\theta\ , \\ \dot{\theta} &= \omega_2 = k_2\ v\ f\sin\phi\ (\frac{1}{d_3} - \frac{1}{d_4}) = k_2\ v\ f\sin\phi\ \left[\frac{\sin(\theta+\phi)}{y+\delta\sin\theta} + \frac{\sin(\theta-\phi)}{\epsilon - y - \delta\sin\theta}\right]\ . \end{aligned} \tag{36}$$

The linearization of the closed–loop system is

$$\dot{z} = A_1(v)\ z \stackrel{\text{def}}{=} \begin{pmatrix} 0 & v \\ -k_2 v\alpha_3 & k_2 v\alpha_4 \end{pmatrix} z\ , \tag{37}$$

where $z \stackrel{\text{def}}{=} (z_2, z_3)$, $\alpha_3 \stackrel{\text{def}}{=} 8f\frac{\sin^2\phi}{\epsilon^2} > 0$ and $\alpha_4 \stackrel{\text{def}}{=} 4f\frac{\sin\phi}{\epsilon^2}(\epsilon\cos\phi - 2\delta\sin\phi)$. Assume that $\epsilon\cos\phi - 2\delta\sin\phi > 0$, thus $\alpha_4 > 0$ (this is true in particular when $\delta = 0$). (N.B. we suppose that $\phi \in (0,\ \frac{\pi}{2})$).

In 37 we replace differentiation with respect to time t by differentiation with respect to the variable s defined by $\dot{s} \stackrel{\text{def}}{=} \frac{ds}{dt} = |v(t)|$. Since v is piecewise continuous, bounded and negative at all times, s is strictly monotonic. Therefore, for a function $f(t)$:

$$\frac{df}{dt} = \frac{df}{ds}\frac{ds}{dt} = \frac{df}{ds}|v|\ . \tag{38}$$

Differentiating z with respect to s, we get from 37 and 38:

$$\frac{dz}{ds} = A_2\ z \stackrel{\text{def}}{=} \begin{pmatrix} 0 & -1 \\ k_2\alpha_3 & -k_2\alpha_4 \end{pmatrix} z\ , \tag{39}$$

The corresponding characteristic polynomial is

$$\det(s\mathit{I\!I} - A_2) = s^2 + k_2\alpha_4 s + k_2\alpha_3\ . \tag{40}$$

The elements of the first column of the Routh array are 1, $k_2\alpha_4$, $k_2\alpha_3$, all of which are positive. Thus, all roots of the characteristic polynomial are in the left half plane.

Therefore, from Lyapunov's indirect method, the system 36 is asymptotically stable around $(y_\star,\ \theta_\star)$.

∎

The natural undamped frequency of 39 is $\omega_n = \sqrt{k_2\alpha_3}$ and its damping ratio is $\zeta = \sqrt{k_2}\frac{\alpha_4}{2\sqrt{\alpha_3}}$. Critical damping is achieved for $\zeta = 1$, thus for

$$k_2 = \frac{4\alpha_3}{\alpha_4^2} = \frac{2\epsilon^2}{f(\epsilon\cos\phi - 2\delta\sin\phi)^2}\ . \tag{41}$$

Proposition 5 *(Instability when $v(t) < 0$)*

Assume that the heading speed v of the unicycle 7 is strictly positive and constant. The angular velocity ω_2 of 35 makes the subsystem 23 of the unicycle kinematics unstable.

Proof

As in the previous proof, after linearization of the closed–loop system 36, we obtain the linear system 37. However, since we now consider constant v, this is a time–invariant system. Its characteristic polynomial is

$$\det(s\mathit{I\!I} - A_1) = s^2 - k_2 v \alpha_4 s + k_2 v^2 \alpha_3 \ . \tag{42}$$

The elements of the first column of the Routh array are 1, $-k_2 v \alpha_4$ (< 0), $k_2 v^2 \alpha_3$ (> 0). There are two sign changes in these elements, thus there are two roots of the characteristic polynomial with positive real parts. Therefore, from Lyapunov's indirect method, the system 36 is unstable.

∎

Up to this point, we considered control laws for the case that the heading speed v is time–varying, but either strictly positive or strictly negative. It is of interest to extend these results to the case when v is allowed to cross zero. However, the previous input scaling procedure cannot be used, in this case, to demonstrate asymptotic stability of the subsystem 23 of the unicycle kinematics.

The control law ω that we consider, when $v(t)$ is allowed to cross zero, consists of applying the angular velocity ω_1 of 27 when $v(t) \geq 0$ and switching to ω_2 of 35 when $v(t) < 0$. Choosing $k_1 = k_2 = k$, the control law ω is

$$\omega = \begin{cases} -k\ \mathcal{L}_1^{1,2}\ , & \text{if } v(t) \geq 0, \\ -k\ \mathcal{L}_1^{3,4}\ , & \text{otherwise.} \end{cases} \tag{43}$$

We first establish by Lyapunov's indirect method that, if the linearization of the closed–loop system corresponding to the control 43 is uniformly asymptotically stable, then so is the subsystem 23. However, the linearized system is now time–varying and no general results exist for establishing its uniform asymptotical stability, except in special cases.

We consider, then, the case when $v(t)$ is time–periodic. We establish that the linearization of the closed–loop system corresponding to the control 43 is exponentially (thus uniformly asymptotically) stable, provided that its solution varies slower than the periodic excitation $v(t)$. Therefore, in this case, the subsystem 23 is also uniformly asymptotically stable.

Proposition 6 *Let the heading speed v of the unicycle 7 be time–varying and assume that it is continuous and bounded. Let $(y,\ \theta) \in (0,\ \epsilon) \times (-\frac{\pi}{2}, \frac{\pi}{2})$. The linearization of the closed–loop system under the switching control law 43 is*

$$\dot{x}(t) = A(t)\ x(t)\ , \tag{44}$$

where $x_1 \stackrel{\text{def}}{=} y - y_\star$, $x_2 \stackrel{\text{def}}{=} \theta - \theta_\star$ and $A(t) \stackrel{\text{def}}{=} \begin{pmatrix} 0 & v \\ -k\alpha_1 v & -k(\alpha_2\ v + \alpha_3\ |v|) \end{pmatrix}$, with $\alpha_1 \stackrel{\text{def}}{=} 8 f \frac{\sin^2\phi}{\epsilon^2} > 0$, $\alpha_2 \stackrel{\text{def}}{=} 8 f \frac{\sin^2\phi}{\epsilon^2} \delta \geq 0$, $\alpha_3 \stackrel{\text{def}}{=} 4 f \frac{\sin\phi\cos\phi}{\epsilon} > 0$. (N.B. we suppose that $\phi \in (0,\ \frac{\pi}{2})$

). This control law stabilizes uniformly asymptotically over $[0, \infty)$ *the subsystem 23 of the unicycle kinematics to* $(y_\star,\ \theta_\star)$*, provided that the corresponding linearized system 44 is also uniformly asymptotically stable over* $[0,\ \infty)$.

Proof

The controls ω_1 and ω_2 of 27 and 35 can be expressed as

$$\begin{aligned} \omega_1 &= -k_1\beta_1(y,\theta)v - k_1\beta_2(y,\theta)|v| \ , \quad \text{when } v \geq 0 \ , \\ \omega_2 &= -k_2\beta_1(y,\theta)v - k_2\beta_2(y,\theta)|v| \ , \quad \text{when } v < 0 \ , \end{aligned} \tag{45}$$

with $k_1,\ k_2 > 0$ and with

$$\begin{aligned} \beta_1(y,\theta) &\stackrel{\text{def}}{=} \frac{1}{2}\Big(\frac{1}{d_1} - \frac{1}{d_2} - \frac{1}{d_3} + \frac{1}{d_4}\Big) = \frac{f\sin^2\phi\cos\theta[2(y+\delta\sin\theta)-\epsilon]}{(\epsilon - y - \delta\sin\theta)(y+\delta\sin\theta)} \ , \\ \beta_2(y,\theta) &\stackrel{\text{def}}{=} \frac{1}{2}\Big(\frac{1}{d_1} - \frac{1}{d_2} + \frac{1}{d_3} - \frac{1}{d_4}\Big) = \frac{f\sin\phi\cos\phi\ \epsilon\ \sin\theta}{(\epsilon - y - \delta\sin\theta)(y+\delta\sin\theta)} \ . \end{aligned} \tag{46}$$

From this, and choosing $k_1 = k_2 = k > 0$, the switching control law ω of equation 43 can be expressed as

$$\omega = -k\ \beta_1(y,\theta)\ v - k\ \beta_2(y,\theta)\ |v| \ , \tag{47}$$

with $\beta_1(y,\theta)$ and $\beta_2(y,\theta)$ as above.

The closed–loop system is then

$$\begin{aligned} \dot{y} &= v\sin\theta \ , \\ \dot{\theta} &= \omega = -k\ \beta_1(y,\theta)\ v - k\ \beta_2(y,\theta)\ |v| \ . \end{aligned} \tag{48}$$

Applying the coordinate transformation

$$x_1 \stackrel{\text{def}}{=} y - y_\star = y - \frac{\epsilon}{2} \ , \quad x_2 \stackrel{\text{def}}{=} \theta - \theta_\star = \theta \ , \tag{49}$$

the system equilibrium is moved to $x = 0$. The closed–loop system becomes

$$\dot{x} = f(t,x) \stackrel{\text{def}}{=} \begin{pmatrix} v(t)\sin x_2 \\ -k\ \beta_1(x)\ v(t) - k\ \beta_2(x)\ |v(t)| \end{pmatrix} \tag{50}$$

where

$$\beta_1(x) \stackrel{\text{def}}{=} \alpha_1 \frac{(x_1 + \delta\sin x_2)\cos x_2}{1 - \frac{4}{\epsilon^2}(x_1 + \delta\sin x_2)^2} \ , \quad \beta_2(x) \stackrel{\text{def}}{=} \alpha_3 \frac{\sin x_2}{1 - \frac{4}{\epsilon^2}(x_1 + \delta\sin x_2)^2} \ . \tag{51}$$

Notice that $f(t,0) = 0$ and that $f(t,x)$ is continuously differentiable with respect to its second argument.

The Jacobian $\frac{\partial f}{\partial x}$ is

$$\frac{\partial f}{\partial x}(t,x) = \begin{pmatrix} 0 & v\cos x_2 \\ -k[\frac{\partial \beta_1}{\partial x_1}(x)v(t) + \frac{\partial \beta_2}{\partial x_1}(x)|v(t)|] & -k[\frac{\partial \beta_1}{\partial x_2}(x)v(t) + \frac{\partial \beta_2}{\partial x_2}(x)|v(t)|] \end{pmatrix} . \tag{52}$$

Define

$$A(t) \stackrel{\text{def}}{=} \left[\frac{\partial f}{\partial x}(t,x)\right]_{x=0} = \begin{pmatrix} 0 & v \\ -k\alpha_1 v & -k(\alpha_2\ v + \alpha_3\ |v|) \end{pmatrix} , \tag{53}$$

where, for $\phi \in (0,\ \frac{\pi}{2})$:

$$\alpha_1 \stackrel{\text{def}}{=} \frac{\partial \beta_1}{\partial x_1}(0) = 8f\frac{\sin^2\phi}{\epsilon^2} > 0 , \quad \alpha_2 \stackrel{\text{def}}{=} \frac{\partial \beta_1}{\partial x_2}(0) = 8f\frac{\sin^2\phi}{\epsilon^2}\delta \geq 0 ,$$
$$\alpha_3 \stackrel{\text{def}}{=} \frac{\partial \beta_2}{\partial x_2}(0) = 4f\frac{\sin\phi\cos\phi}{\epsilon} > 0 . \tag{54}$$

The linearization of the nonlinear system 48 is the time–varying linear system

$$\dot{x}(t) = A(t)\ x(t) , \tag{55}$$

for the matrix $A(t)$ defined above.

Since v is bounded, $v_1 < v(t) < v_2$, for all $t \geq 0$ and for some $v_1,\ v_2 \in I\!R$. Then, $0 \leq |v(t)| < v_3 \stackrel{\text{def}}{=} \max\{v_1,\ v_2\}$. Thus, $A(t)$ is also bounded.

Define

$$f_1(t,\ x) \stackrel{\text{def}}{=} f(t,\ x) - A(t)\ x = \begin{pmatrix} v\ (\sin x_2 - x_2) \\ -k\ [\beta_1(x) - \alpha_1\ x_1 - \alpha_2\ x_2]\ v - k\ [\beta_2(x) - \alpha_3\ x_2]\ |v| \end{pmatrix} . \tag{56}$$

It is easy to see that

$$\sup_{t\geq 0}\frac{||f_1(t,\ x)||}{||x||} = v_3\left[\frac{(\sin x_2 - x_2)^2 + k^2(|\beta_1(x) - \alpha_1\ x_1 - \alpha_2\ x_2| + |\beta_2(x) - \alpha_3\ x_2|)^2}{x_1^2 + x_2^2}\right]^{\frac{1}{2}} .$$

By series expansion of the quantities $\beta_1(x) - \alpha_1\ x_1 - \alpha_2\ x_2$ and $\beta_2(x) - \alpha_3\ x_2$, it can be seen that both contain only terms proportional to $x_1^3,\ x_1^2\ x_2,\ x_1\ x_2^2,\ x_2^3$ and higher order terms in x_1 and x_2. Since $|x_1|,\ |x_2| \leq ||x||$, then $|\beta_1(x) - \alpha_1\ x_1 - \alpha_2\ x_2| \leq \gamma_1||x||^3 + (h.o.t.\ in\ ||x||)$ and $|\beta_2(x) - \alpha_3\ x_2| \leq \gamma_2||x||^3 + (h.o.t.\ in\ ||x||)$, for some $\gamma_1,\ \gamma_2 > 0$. Then

$$\sup_{t\geq 0}\frac{||f_1(t,\ x)||}{||x||} \leq v_3\left[\frac{||x||^6 + (h.o.t.\ in\ ||x||)}{||x||^2}\right]^{\frac{1}{2}} = v_3||x||^2\left[1 + (h.o.t.\ in\ ||x||)\right]^{\frac{1}{2}} .$$

Therefore

$$\lim_{||x||\to 0}\sup_{t\geq 0}\frac{||f_1(t,\ x)||}{||x||} = 0 .$$

Thus, from Lyapunov's indirect method, the result follows.

■

Proposition 7 *(Periodic v)*

Assume that the heading speed v is (i) time–periodic with period $T > 0$ (i.e. $v(t + T) = v(t)$), (ii) continuous, (iii) there exists a $T_1 \in [0,\ T)$ such that $|v(T_1)| > 0$ and (iv) $\int_0^T v(\sigma)d\sigma \neq 0$. Assume further that $\alpha_3 > \alpha_2$, for the quantities defined in 54. Then, there exists an $\alpha_0 > 0$, such that the zero solution of

$$\dot{z}(t) = A(\alpha\ t)\ z(t)\ , \tag{57}$$

where $A(t)$ is the matrix defined in 53, is uniformly asymptotically stable over $[0, \infty)$, for all $\alpha > \alpha_0$.

Proof

The matrix $A(t)$ is obviously time–periodic with period T. Consider

$$\bar{A} \stackrel{\text{def}}{=} \frac{1}{T}\int_0^T A(\sigma)d\sigma = \begin{pmatrix} 0 & v_I \\ -k\ \alpha_1\ v_I & -k\ (\alpha_2\ v_I + \alpha_3\ v_{II}) \end{pmatrix}\ , \tag{58}$$

where $v_I \stackrel{\text{def}}{=} \frac{1}{T}\int_0^T v(\sigma)d\sigma$ and $v_{II} \stackrel{\text{def}}{=} \frac{1}{T}\int_0^T |v(\sigma)|d\sigma$. The characteristic polynomial of $\bar{A}$ is

$$\det(s\mathbb{I} - \bar{A}) = s^2 + k\ (\alpha_2\ v_I + \alpha_3\ v_{II})s + k\alpha_1 v_I^2\ . \tag{59}$$

When $\alpha_3 > \alpha_2$, we have $\alpha_2\ v(t) + \alpha_3\ |v(t)| \geq 0$, for all $t \in [0,\ T)$. Since there exists at least one $T_1 \in [0,\ T)$ such that $|v(T_1)| > 0$, then $\alpha_2\ v(T_1) + \alpha_3\ |v(T_1)| > 0$, thus $\int_0^T [\alpha_2\ v(t) + \alpha_3\ |v(t)|]dt > 0$, therefore, $\alpha_2\ v_I + \alpha_3\ v_{II} > 0$. Also, $v_{II} > 0$. When $\int_0^T v(t)dt \neq 0$, then $k\ \alpha_1\ v_I^2 > 0$. Thus, all coefficients of the characteristic polynomial of $\bar{A}$ are strictly positive and, from the Routh–Hurwitz test, all eigenvalues of $\bar{A}$ have strictly negative real part.

The exponential stability of 57 follows from a classical averaging result (Brockett [3], Khalil [12]). For linear systems, exponential stability is equivalent to uniform asymptotic stability.

∎

5 Simulation Results

Fig. 3 shows MATLAB simulations where the heading speed varies sinusoidally and the control 24 with gains $k_1 = 1$ and $k_2 = 1.4142$ achieves stabilization of (y, θ) to the desired values $(y_\star = 5,\ \theta_\star = 0)$ starting from the initial values $(y = 4,\ \theta = 0.4)$. The model parameters are $\epsilon = 10,\ f = 1,\ \delta = 1,\ \phi = \frac{\pi}{4}$. The state (y, θ) is being reconstructed at each time instant from panoramic visual data.

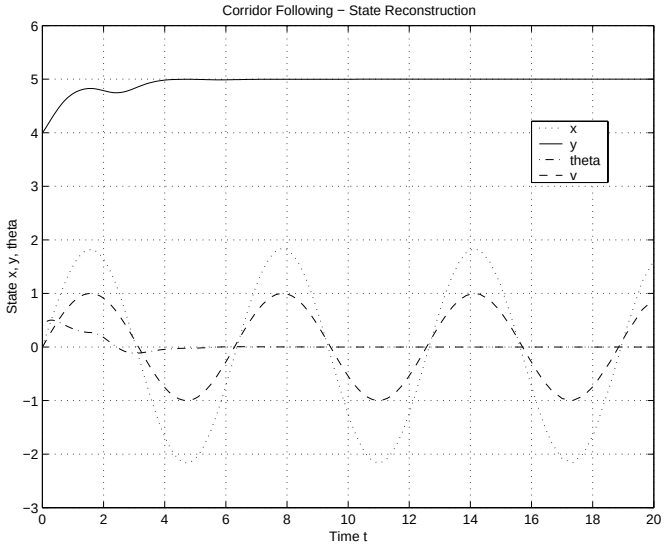

Figure 3: Corridor following with reconstruction of state

Figures 4 and 5 show MATLAB simulations, analogous to the ones in fig. 3, but using the controls 27 and 35 with gains $k_1 = k_2 = 1.4$. The heading speed is time–varying, but, respectively, strictly positive and strictly negative (e.g. in fig. 4, the heading speed is $v(t) = 1 + 0.4 \sin t$). The model parameters are $\epsilon = 10,\ f = 1,\ \delta = 1,\ \phi = \frac{\pi}{4}$. The state (y, θ) **is not** being reconstructed in this case.

Fig. 6 shows MATLAB simulations of the system, where the heading speed of the mobile robot varies periodically with time $(v(t) = 0.1 + \sin t + \sin \frac{t}{2})$. The model parameters are $\epsilon = 10,\ f = 1,\ \delta = 0,\ \phi = \frac{\pi}{4}$. The switching control 43 with gain $k = 4$ is used to achieve stabilization of (y, θ) to the desired values $(5,\ 0)$ starting from the initial state $(4,\ 0.4)$.

Fig. 7 shows the behavior of control 27 in a more complicated environment.

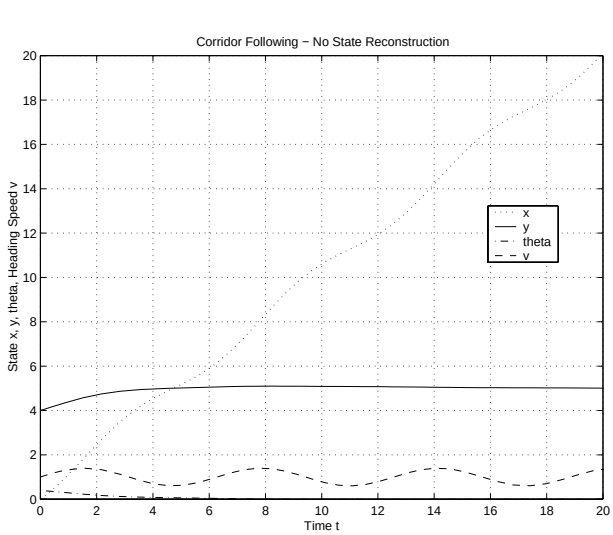

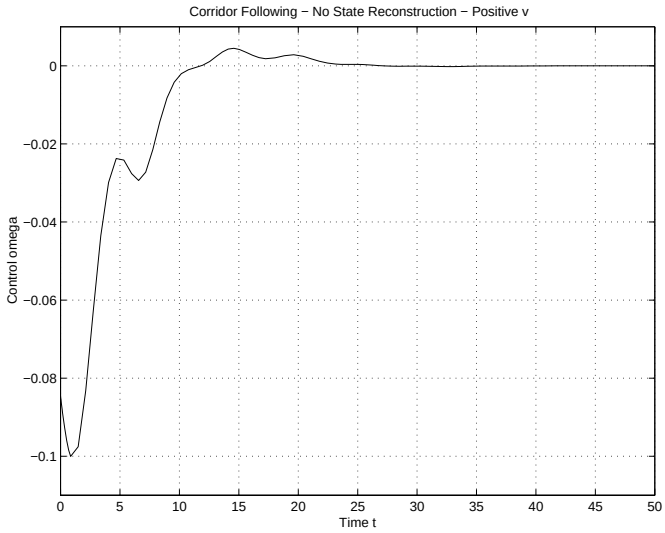

(a) State $(x,\ y,\ \theta)$ and heading speed v (b) Control ω_1

Figure 4: Corridor following without reconstruction of state: Positive v

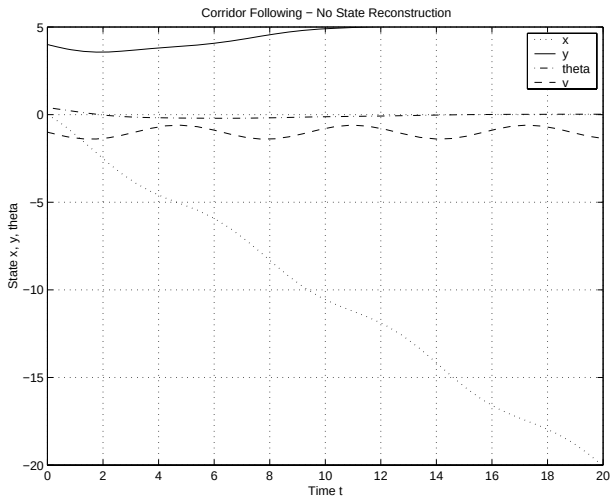

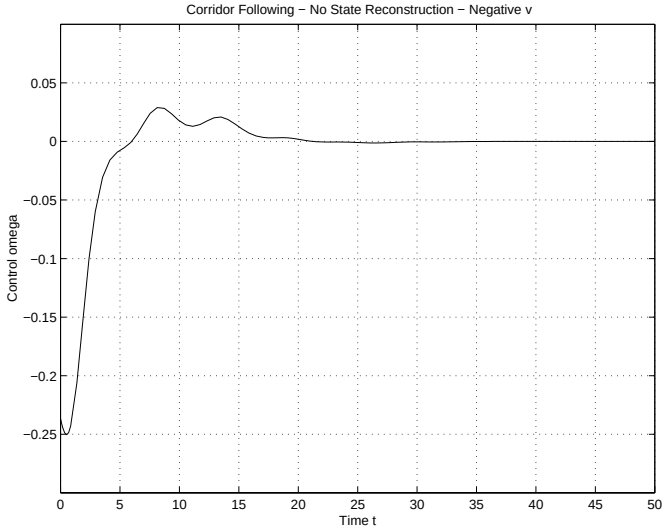

(a) State $(x,\ y,\ \theta)$ and heading speed v (b) Control ω_2

Figure 5: Corridor following without reconstruction of state: Negative v

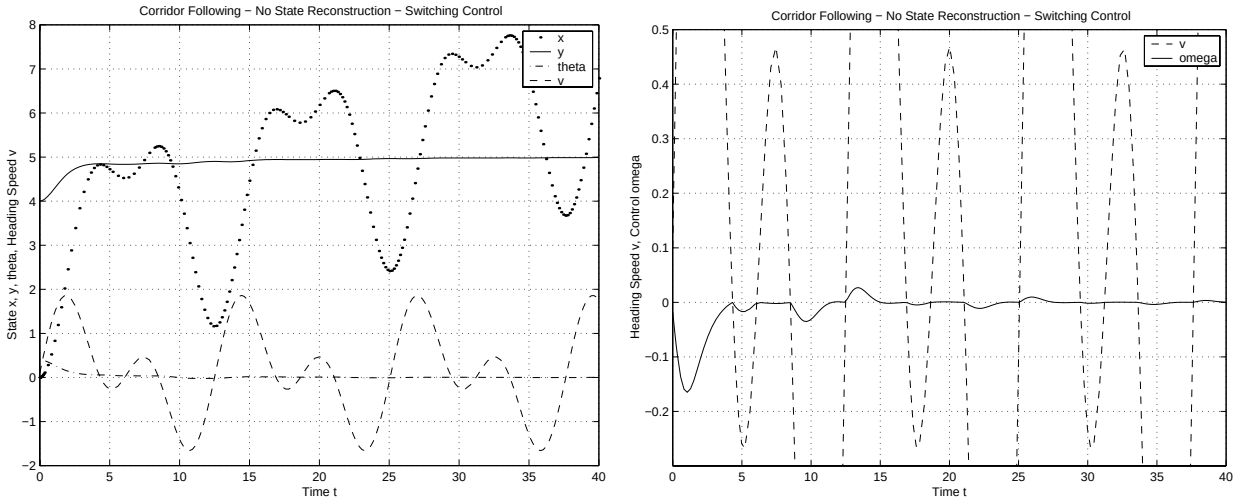

(a) State $(x,\ y,\ \theta)$ and heading speed v (b) Switching control ω and heading speed v

Figure 6: Corridor Following: Time–Periodic $v(t)$ and Switching Control $\omega(t)$

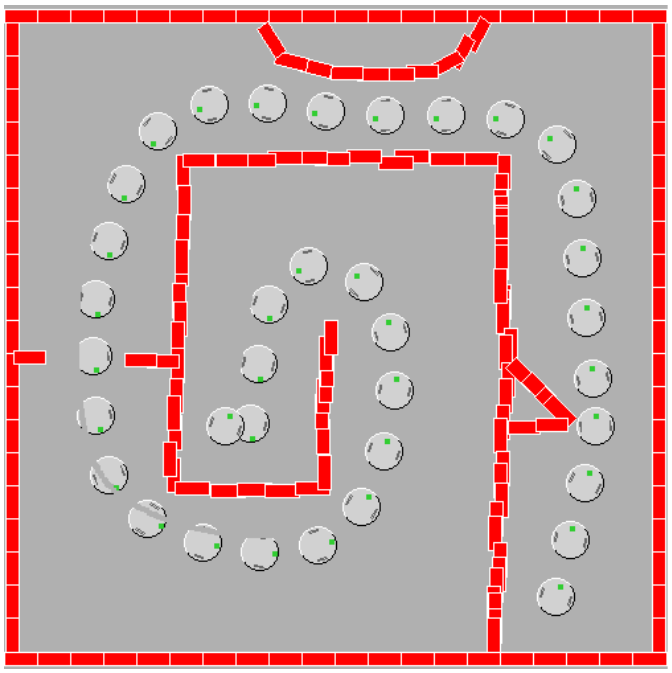

Figure 7: Corridor following without reconstruction of state

6 Experimental Results

Experiments evaluating the proposed techniques were performed at the Computer Vision and Robotics lab of ICS–FORTH. The preliminary results contained in this report are based on the use of laser as a sensory modality and aim at demonstrating the performance of controls of the type of those in equations 27 and 25, i.e.

$$\omega = -k\ v \sin\phi\ (\frac{1}{d_1} - \frac{1}{d_2}) \tag{60}$$

when $v > 0$, in accomplishing the corridor–following task. The laser is used to measure directly the distances d_1 and d_2 from the walls, a task that will become unnecessary when panoramic vision is used.

(a) Mobile robot (b) Panoramic camera

Figure 8: Mobile robot with panoramic camera and laser

The experiments were performed with the RWI B21r robot of CVRL, which is equipped with a SICK laser range finder, covering 180 degrees of the robot's surroundings at an angular resolution of 0.5 degrees and at a distance resolution of 0.5 cm. The robot is also equipped with a panoramic camera, which will be used in subsequent experiments. In order to support processing of sensory information, control of the platform and communication with the external world, the robot is equipped with two PENTIUM III–based on-board computers running at 800 MHz. Each of these computers is equipped with 256 Mbytes of

RAM and operates under the LINUX operating system. To communicate with the rest of the world, a 2.4 GHz four–port Ethernet radio pair with antennas (100mW) has been installed providing a data rate of 3 Mbits/sec.

In this experiment, the robot moves in a straight corridor, approximately 3 m. wide, with a heading speed of 0.12 m/sec. The gain k of the control 60 is 1.25. Fig. 9 shows the raw laser data d_1 and d_2 taken at the directions $\phi = \pm\frac{\pi}{4}$, with respect to the heading direction, during the experiment. The data are taken at a rate of about 2 samples/sec. Notice that after about 60 sec (120 samples), the two distances become equal, designating motion in the middle of the corridor.

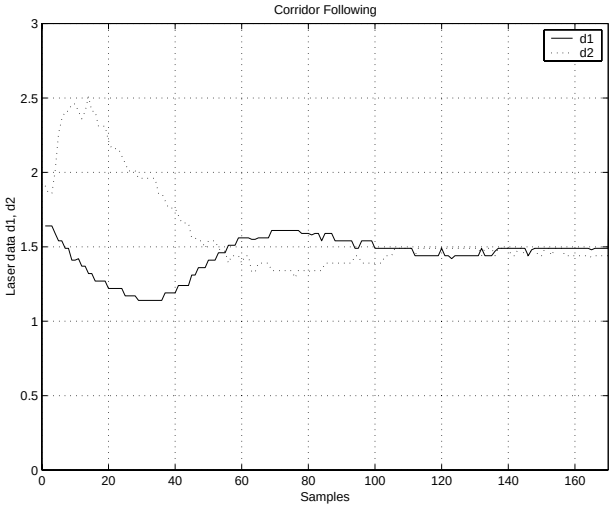

Figure 9: Laser data during the experiment

The robot starts from the initial configuration $(y,\ \theta) = (0.44\ m,\ 0.56\ rad)$ and arrives at the desired configuration $(y_\star,\ \theta_\star) = (1.5\ m,\ 0.0\ rad)$ after about 60 sec, as it can be seen in fig. 10.b. This figure shows the state of the robot, which is reconstructed from the laser data. This reconstructed state *is not* used in the control of the robot however.

Fig. 10.a shows the evolution of the control ω during the experiment.

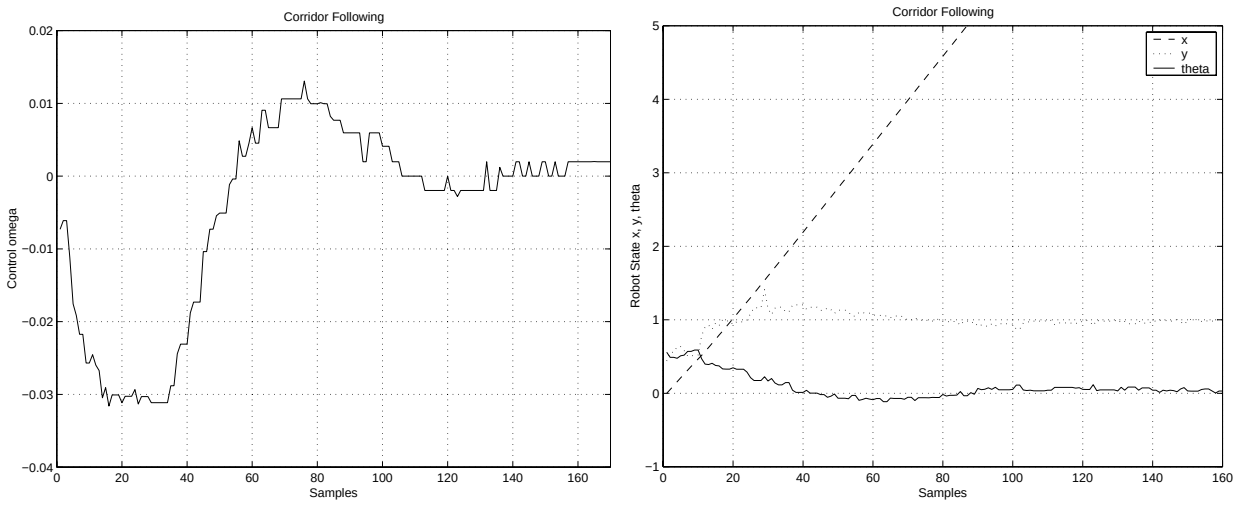

(a) Control ω (b) State x, y, θ

Figure 10: Mobile robot control and state during the experiment

7 Conclusions

A framework was presented for the utilization of data from panoramic images to the task of corridor following by a mobile robot. The visual servoing–type schemes derived were shown to possess the required stability properties. Future work will focus on the experimental evaluation of these techniques, which is currently in progress.

Acknowledgments

This work was partially supported by the European Commission through project TOURBOT, contract No. IST-1999-12643, under the IST program, and by the General Secretariat for Research and Technology of the Hellenic Ministry of Development through project DRIVER, contract No. 98AMEA 18. The contributions of K. Hatzopoulos in the experimental part of this work is gratefully acknowledged.

References

[1] A.A. Argyros and F. Bergholm, "Combining Central and Peripheral Vision for Reactive Robot Navigation", Proc. Computer Vision and Pattern Recognition Conf. (CVPR'99), Fort Collins, Colorado, USA, June 23-25, 1999.

[2] J.L. Barron, D.J. Fleet and S.S. Beauchemin, "Performance of Optical Flow Techniques", *Intl. J. Computer Vision* **12:1**, 43-77, 1994.

[3] R.W. Brockett, *Finite Dimensional Linear Systems*, John Wiley and Sons, Inc., 1970.

[4] C. Canudas de Wit, B. Siciliano and G. Bastin Eds., *Theory of Robot Control*, Springer–Verlag, 1996.

[5] T. Collett, "Measuring Beelines to Food", *Science* **287**, 817-818, 2000.

[6] B. Espiau, F. Chaumette and P. Rives, "A New Approach to Visual Servoing in Robotics", *IEEE Trans. on Robotics and Automation* **8**, 313-326, 1992.

[7] C. Fermüller and Y. Aloimonos, "Geometry of Eye Design: Biology and Technology", Center for Automation Research Technical Report CAR-TR-900, University of Maryland, College Park, USA, 15 pages, 1998.

[8] J. Gaspar and J. Santos–Victor, "Visual Path Following with a Catadioptric Panoramic Camera", Proc. 7th Intl. Symposium on Intelligent Robotic Systems (SIRS'99), Coimbra, Portugal, July 1999 (also VisLab TR 05/99).

[9] G.D. Hager and S. Hutchinson, Eds., "Vision–based Control of Robotic Manipulators", Special section of *IEEE Trans. Robotics and Automation* **12**, 649-774, 1996.

[10] E.C. Hildreth, "The Computation of the Velocity Field", *Proc. R. Soc. Lond.* **B 221**, 189-220, 1984.

[11] B.K.P. Horn, *Robot Vision*, Mc Graw–Hill, 1986.

[12] H.K. Khalil, *Nonlinear Systems*, Macmillan Publishing Co., 1992.

[13] S.K. Nayar and S. Baker, "A Theory of Catadioptric Image Formation", Technical Report CUCS-015-97, 30 pages, Dept. of Computer Science, Columbia University, 1997.

[14] J. Santos–Victor, G. Sandini, F. Curotto and S. Garibaldi, "Divergent Stereo for Robot Navigation: Learning from Bees", IEEE Intl. Conf. on Computer Vision and Pattern Recognition (CVPR'93), New York, USA, June 1993.

[15] J. Santos–Victor, G. Sandini, F. Curotto and S. Garibaldi, "Divergent Stereo in Autonomous Navigation: From Bees to Robots", *Intl. J. of Computer Vision* **14**, 159-177, 1995.

[16] C. Samson, "Path Following and Time–Varying Feedback Stabilization of a Wheeled Mobile Robot", Proc. 2nd Intl. Conf. on Automation, Robotics and Computer Vision (ICARCV'92), Singapore, 1992.

[17] C. Samson, "Control of Chained Systems: Application to Path Following and Time–Varying Point–Stabilization of Mobile Robots", *IEEE Trans. on Automatic Control* **40**, 64-77, 1995.

[18] M.V. Srinivasan, S. Zhang, M. Altwein and J. Tautz, "Honeybee Navigation: Nature and Calibration of the 'Odometer' ", *Science* **287**, 851-853, 2000.

[19] T. Svoboda, T. Pajdla and V. Hlavac, "Epipolar Geometry for Panoramic Cameras", Proc. 5th European Conf. on Computer Vision, pp. 218–232, LNCS 1406, Springer–Verlag, 1998.

[20] D.P. Tsakiris, P. Rives and C. Samson, "Applying Visual Servoing Techniques to Control Nonholonomic Mobile Robots", Proc. Workshop on "New Trends in Image–based Robot Servoing", Eds. R. Horaud and F. Chaumette, IEEE/RSJ International Conference on Intelligent Robots and Systems (IROS'97), pp. 21-32, Grenoble, France, September 8-12, 1997.

[21] D.P. Tsakiris, P. Rives and C. Samson, "Extending Visual Servoing Techniques to Nonholonomic Mobile Robots", in *The Confluence of Vision and Control*, Eds. G. Hager, D. Kriegman and S. Morse, Lecture Notes in Control and Information Systems (LNCIS 237), Springer-Verlag, 1998.

[22] M. Vidyasagar, *Nonlinear Systems Analysis*, Prentice–Hall, 1978.